IEEE Access
Multidisciplinary : Rapid Review : Open Access Journal

Received 22 September 2023, accepted 20 October 2023, date of publication 30 October 2023, date of current version 3 November 2023.

Digital Object Identifier 10.1109/ACCESS.2023.3328534

RESEARCH ARTICLE

Low-Artifact and Fast Backlit Image Enhancement Method Based on Suppression of Lightness Order Error

MASATO AKAI[1], YOSHIAKI UEDA[2], (Member, IEEE), TAKANORI KOGA[3], (Member, IEEE), AND NORIAKI SUETAKE[4], (Member, IEEE)

[1]Imaging Solution Development Department, Nikon Corporation, Minato-ku, Tokyo 108-6290, Japan
[2]Faculty of Advanced Science and Technology, Ryukoku University, Otsu-shi, Shiga 520-2194, Japan
[3]Faculty of Humanity-Oriented Science and Engineering, Kindai University, Iizuka-shi, Fukuoka 820-8555, Japan
[4]Graduate School of Science and Technology for Innovation, Yamaguchi University, Yamaguchi-shi, Yamaguchi 753-8512, Japan

Corresponding author: Noriaki Suetake (suetake@sci.yamaguchi-u.ac.jp)

ABSTRACT Many image enhancement methods have been proposed to improve the visibility of backlit images. Although these methods can effectively improve the visibility of the subject and background compared to standard image enhancement methods, they may result in image quality degradation owing to non-negligible artifacts. In many cases, such artifacts are caused by a significant change in the Lightness Order Error (LOE) between the original and processed images. To address this problem, this paper proposes a low-artifact and fast backlit image enhancement method to effectively improve the visibility of images by suppressing the LOE. The proposed method uses adaptive luminance correction to generate lightness-enhanced images of the dark and bright areas of the backlit image. These images are then fused based on a weight map to calculate the lightness of the output image with a lower LOE. The final output, i.e., the enhanced color image, is obtained by multiplying the input color image by the ratio of the lightness component of the input image to the enhanced lightness component. The experimental results demonstrate the superiority of the proposed method in terms of low artifacts, natural enhancement, and high processing speed based on straightforward processing.

INDEX TERMS Backlit image, image enhancement, lightness order error, low-artifact image.

I. INTRODUCTION

In a video or a photograph taken under backlighting conditions, i.e., a backlit image, the subject's background is affected by the light source, and the foreground subject is in shadow, resulting in extremely dark and bright areas being included in the same image. Digital cameras for general use do not have a high dynamic range to represent the difference between dark and bright patterns within each of extremely dark and bright areas in a backlit image [1]. Owing to this low dynamic range, the lightness values of many pixels in backlit images are extremely low in dark areas and extremely high in bright areas. Therefore, the visibility of the subject and background in a backlit image is significantly reduced. The reduced visibility of the subject and background in dark and bright areas in a backlit image may lead to the overall performance degradation of outdoor surveillance and in-vehicle camera systems, which often acquire images under backlighting conditions. In recent years, such image processing systems, especially for segmentation, object recognition, and scene analysis, are often implemented on embedded hardware using computational intelligence. Hence, as pre-processing so that the computational intelligence for those applications can see the images better, it is crucial to realize a fast enhancement process that improves the visibility of subjects and backgrounds by improving the contrast between the dark and bright areas in backlit images.

To improve the visibility of subjects and backgrounds in backlit images, various problems arise when general image enhancement techniques are applied [2], [3], [4].

The associate editor coordinating the review of this manuscript and approving it for publication was Larbi Boubchir.

When applying the gamma correction to backlit images, enhancing the dark areas saturates the bright areas, and enhancing the bright areas further darkens the dark areas. Histogram equalization (HE) and contrast-limited adaptive histogram equalization (CLAHE) [5] are the frequently used contrast enhancement methods. However, when applied to backlit images, these methods cause a significant degradation of image quality owing to over-enhancement. Single-scale retinex (SSR) [6] and Multiscale retinex with color restoration (MSRCR) [7] are frequently used retinex theory-based image enhancement methods. However, when applied to backlit images, they often cause a significant degradation of image quality owing to halos. Thus, these general image enhancement methods cannot effectively improve the visibility of backlit images.

In addition to the problems mentioned above, since the lighting conditions at the time of image shooting are not always sufficient and are often non-uniform, many retinex-based methods have been proposed to enhance images captured under various lighting conditions [8], [9], [10]. Wang et al. proposed a method named "naturalness-preserving enhancement algorithm (NPEA)," [8] which uses a brightness-pass filter and bi-log transformation to deal with non-uniform lighting conditions. Guo et al. proposed a retinex-based image enhancement method for low-light images named LIME [9]. The method creates an illumination map for each pixel using the maximum value of the R, G, and B channels and refines the map based on the structure prior to achieving high-quality image enhancement. While these methods can achieve high-quality enhancement for various types of images, it cannot be ignored that retinex-based methods may cause white skipping, blacking out, excessive brightness enhancement, and color reproduction problems.

In contrast, Wang et al. [11], Fu et al. [12], and Buades et al. [13] proposed enhancement methods suitable for backlit images based on image fusion. The method of Wang et al. generates three lightness-transformed images from an input lightness image and uses the fusion method in [14] to obtain the output image. The log function, gamma correction, and unsharp masking [15] are used to generate the three lightness-transformed images. This method can effectively improve visibility in dark areas but may produce roughness and artifacts in bright areas. Fu et al. proposed a method that uses illumination estimation by morphological closing, brightness enhancement by a sigmoid function, and contrast enhancement by adaptive histogram equalization to obtain relatively good enhancement results. The method of Buades et al. generates multiple exposure images using two types of global tone mapping curves: gamma correction and logarithmic function. The output image is obtained by fusing multiple-exposure images using a modified algorithm in [16] and applying sharpening and chrominance correction. This method improves visibility in dark areas but may generate artifacts, roughness, and highlight clipping in bright areas.

Li et al. [17], Vazquez-Corral et al. [18], and Trongtirakul et al. [19] proposed segmentation-based backlit image enhancement methods. The method of Li et al. identifies underexposed and overexposed regions by soft binary segmentation processing using a Gaussian mixture model (GMM). Then, different tone mappings are applied to each identified region to produce the output image. The method of Vazquez-Corral et al. uses an iterative gradient descent method to generate a set of weight maps. Then, on the basis of weights, multiple tone-mapped images are merged using the method in [20] to obtain the output image. The method of Trongtirakul et al. divides the input lightness image into three regions, namely, underexposed, mid-tone, and overexposed regions, and stretches the contrast in the underexposed and overexposed regions. The image with stretched contrast is then enhanced by locally weighted logarithmic bi-HE, and the images are fused on the basis of a weight function. Li and Wu also proposed a method based on a segmentation process performed by supervised learning [21]. This method uses a segmentation process to detect the subject and then fuse the output results from two tone-mapped images to improve the visibility of the subject and overexposed regions. This method tends to produce artifacts not present in the original image. Furthermore, as mentioned in Lv et al.'s report [22], these segmentation-based methods have long processing times and are unsuitable for high-resolution images.

Another approach, learning-based backlit image restoration, has been proposed by Zhang et al. [23]. Their method uses iterative learning to process the image without prior learning. Specifically, image restoration is performed by deriving a block-based loss function and estimating S-curves for appropriate enhancement. In this method, the S-curve may not be appropriately estimated, and visibility may not be sufficiently improved. Although similar approaches for low-light images have been studied in [24] and [25], the same problem may occur. Furthermore, many large-scale deep-learning-based low-light image enhancement methods [26], [27], [28], [29], [30], [31], [32], [33] have recently been proposed. However, the performance of these data-driven methods depends on the dataset used for training, and they may not be able to adequately cope with various scenes or complex and non-uniform real-world low-light images [34]. In addition, deep learning-based methods tend to have large models, which can cause hardware resource issues, particularly when implemented in real-world applications such as embedded systems. Other new approaches have been adopted in recent years, such as using raw images [35] and tree search [36], but they pose similar resource problems. Therefore, there is still a strong need for handcrafted and straightforward image enhancement algorithms.

As explained above, many conventional enhancement methods for backlit images may produce undesirable structures, such as artifacts and highlight clipping that were not present in the original image. One reason for this

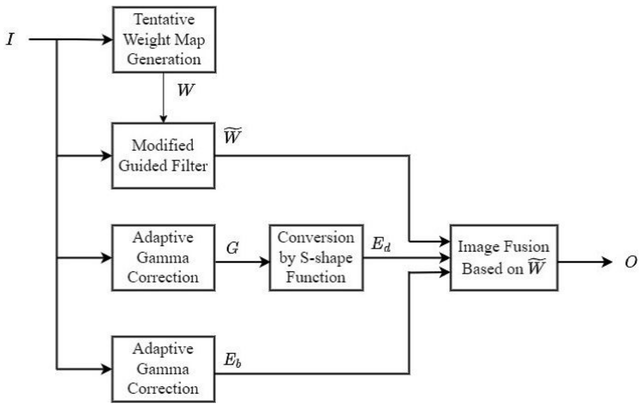

FIGURE 1. Flow of lightness enhancement process.

phenomenon is that the order of lightness changes before and after the enhancement process, resulting in the appearance of dark or bright regions that were not present in the original image. To address this problem, in this paper, we propose a fast enhancement method for backlit images that suppresses the change in the order of lightness in the original image and reduces the occurrence of artifacts.

The remainder of this paper is organized as follows. Section I shows the introduction. In Section II, we describe the proposed algorithm in detail. In Section III, we describe the comparative experiments between the proposed and conventional methods. In the experiments, multiple backlit images were used for qualitative evaluation by visual inspection. Furthermore, quantitative evaluation was conducted using various evaluation indices to verify the effectiveness of the proposed method in artifact reduction. The average computation time and the effect of each parameter in the proposed method were also verified. Finally, Section IV shows the conclusions.

II. PROPOSED METHOD

The proposed method separately generates lightness-enhanced images for the dark and bright areas in backlit images. Then, the lightness of the output image is calculated by fusing these images on the basis of a weight map. Figures 1 and 2 show the flow of the lightness enhancement process and the example images and histograms obtained in the processing flow, respectively. The final output, an enhanced color image $\boldsymbol{O}^c$, is obtained by multiplying the input color image $\boldsymbol{I}^c$ by the ratio of the enhanced lightness component O to the lightness component I of the input image. The enhancement for the dark and bright areas is performed by lightness correction using tone curves to suppress the Lightness Order Error (LOE) [8], [9]. In the lightness correction for the bright areas, a downward-convex adaptive gamma curve is applied to the input lightness image I to obtain a lightness-improved image E_b. For the dark areas, an upward-convex adaptive gamma curve and an S-curve are applied to I to obtain images G and E_d, which are improved in lightness and contrast. In obtaining the weight map using a threshold determined by Otsu's discriminant analysis method [37], I is divided into dark and bright areas. Then, a tentative weight map W is first

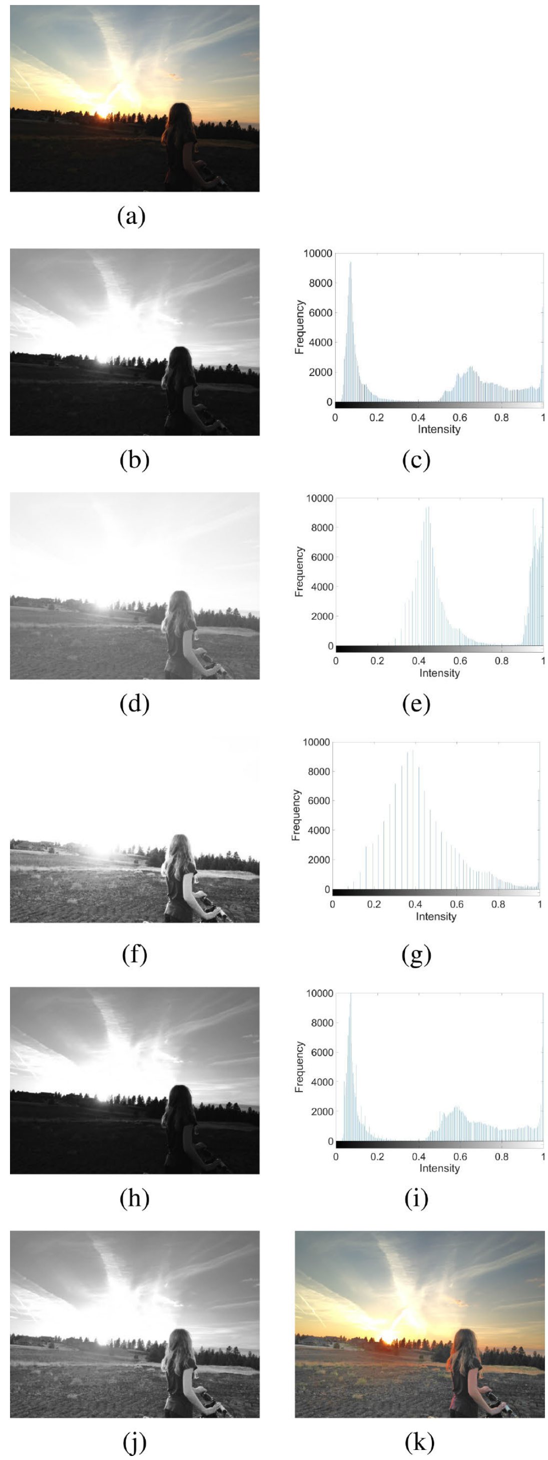

FIGURE 2. Images and histograms in the backlit image enhancement process. (a) Backlit image. (b) Lightness image of (a). (c) Lightness histogram of image (b). (d) Image after lightness correction by the adaptive gamma correction using an upward-convex tone curve. (e) Histogram of image (d). (f) Lightness transformed image using an S-shaped tone curve. (g) Histogram of image (f). (h) Image after lightness correction by the adaptive gamma correction method using a downward-convex tone curve. (i) Histogram of image(h). (j) Enhanced lightness image by the proposed method. (k) Output color image.

generated by weighting only for the dark areas. In this map, the lower the lightness value, the greater the weight, with values ranging from 0 to 1. On the other hand, all weights in the bright areas are 0. To suppress the LOE, an edge-preserving smoothing process is performed for W using a modified version of the guided filter [38] with I as a guide image, and the final weight map $\tilde{W}$ is obtained.

Now, let $\boldsymbol{I}^c(i,j) = (I^{\mathrm{R}}(i,j), I^{\mathrm{G}}(i,j), I^{\mathrm{B}}(i,j))^\top$ $(i = 1, 2, \cdots, M; j = 1, 2, \cdots, N)$ be the pixel value represented in column vector form at the coordinates (i, j) in an $M \times N$ size 24-bit full-color input backlit image. First, each pixel value of the input color image $\boldsymbol{I}^c$ is divided by 255 and normalized to the range [0, 1]. Next, each pixel value $I(i, j)$ of the lightness image of the input color image $\boldsymbol{I}^c$ is calculated as follows:

$$I(i,j) = \max_{c \in \mathrm{R,G,B}} \boldsymbol{I}^c(i,j). \tag{1}$$

Figure 2(a), 2(b), and 2(c) show an example of a backlit image, its lightness image, and its lightness histogram, respectively. As shown in Fig. 2(c), usually, a backlit image has a bimodal pixel distribution [39], and many pixels are biased toward the lower and higher lightness values. This tendency indicates that many pixels have low lightness values in dark areas and high lightness values in bright areas. In such dark and bright areas, the contrast is reduced by the slight difference in lightness between adjacent pixels, significantly reducing the subject and background visibility. Therefore, it is necessary to sufficiently improve the visibility, especially in dark areas with object information, such as the target subject.

A. GENERATION OF A WEIGHT MAP

In the proposed method, a weight map $\tilde{W}$ is generated to fuse two enhanced lightness images E_d and E_b that improve the visibility of dark and bright areas in the input lightness image, respectively. As shown in the histogram in Fig. 2(c), in general, the lightness histograms of backlit images tend to be bimodal. Using this feature, we can determine the threshold t that maximizes the separability between the bimodal lightness distributions of pixels belonging to the dark and bright classes by Otsu's discriminant analysis method as follows:

$$t = \arg\max_{V} \{\omega_1(V)\,\omega_2(V)\,(m_1(V) - m_2(V))^2\}, \tag{2}$$

where V represents an arbitrary threshold for lightness; $\omega_1(V)$ and $\omega_2(V)$ are the numbers of pixels in the dark and bright classes, respectively. Moreover, $m_1(V)$ and $m_2(V)$ are the average lightness values of the pixels belonging to the dark and bright classes, respectively.

Using the determined threshold t, we can generate the tentative weight map W from the input lightness image I as follows:

$$W(i,j) = \begin{cases} 1 - \dfrac{I(i,j)}{t}, & I(i,j) < t \\ 0, & \text{otherwise.} \end{cases} \tag{3}$$

Figure 3(a) shows the tentative weight map W for the image shown in Fig. 2(a). In Fig. 3(a), some edge structures are

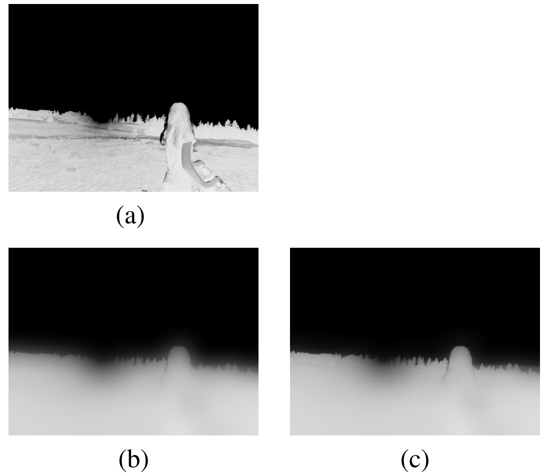

FIGURE 3. Effect of the weight map correction process using the modified guided filter. (a) Tentative weight map before edge-preserving smoothing. (b) Edge-preserving smoothed version of (a) obtained using the original guided filter [38]. (c) Edge-preserving smoothed version of (a) obtained using the modified guided filter.

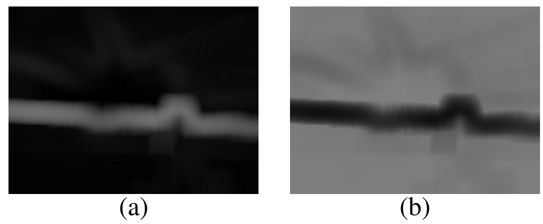

FIGURE 4. Relationship between the local standard deviation and parameter ε. (a) Local standard deviation map. (b) ε map.

visible in the area corresponding to the dark area in the input image. In addition, an enormous edge structure that separates the dark and bright areas in the input image appears at the lower center of the map. This appearance is because Otsu's discriminant analysis method determines the threshold on the basis of the entire lightness distribution in the image without considering local lightness patterns in the input image. The weight map containing many discontinuous pixel values (i.e., edge structures in dark areas) can significantly cause image quality degradation in image enhancement because it significantly changes the lightness order during image fusion.

To address this problem, we apply a correction to the tentative weight map W using a modified version of the guided filter [38] with the input lightness image I as a guide image. To apply the guided filter, $\overline{I}(i,j)$ and $\overline{W}(i,j)$ for each pixel in I and W are first calculated as follows:

$$\overline{I}(i,j) = \frac{1}{n^2} \sum_{(k,l) \in \Omega(i,j)} I(k,l), \tag{4}$$

$$\overline{W}(i,j) = \frac{1}{n^2} \sum_{(k,l) \in \Omega(i,j)} W(k,l), \tag{5}$$

where $\Omega(i,j)$ is a square region of $n \times n$ pixels centered at the coordinates (i, j) and (k, l) denotes the coordinates of the pixels in the square region. Next, the filtering coefficients

$a(i,j)$ and $b(i,j)$ are calculated as follows:

$$a(i,j) = \frac{\frac{1}{n^2} \sum_{(k,l)\in\Omega(i,j)} I(k,l)\cdot W(k,l) - \bar{I}(i,j)\cdot \overline{W}(i,j)}{\sigma(i,j)^2 + \varepsilon}, \tag{6}$$

$$\sigma(i,j) = \frac{1}{n}\sqrt{\sum_{(k,l)\in\Omega(i,j)} \left(I(k,l) - \bar{I}(i,j)\right)^2}, \tag{7}$$

$$b(i,j) = \overline{W}(i,j) - a(i,j)\cdot \bar{I}(i,j), \tag{8}$$

where $\sigma(i,j)$ is a local standard deviation of I and ε is a parameter that controls the edge preservation performance; the smaller the value of ε, the better the edge preservation performance. Subsequently, the output of the filter, that is, the final weight map $\tilde{W}$, is calculated as follows:

$$\tilde{W}(i,j) = \bar{a}(i,j)\cdot I(i,j) + \bar{b}(i,j), \tag{9}$$

$$\bar{a}(i,j) = \frac{1}{n^2}\sum_{(k,l)\in\Omega(i,j)} a(k,l), \tag{10}$$

$$\bar{b}(i,j) = \frac{1}{n^2}\sum_{(k,l)\in\Omega(i,j)} b(k,l), \tag{11}$$

where $\tilde{W}(i,j)$ is a pixel value of the edge-preserving smoothed weight map $\tilde{W}$ at the coordinates (i,j).

Figure 3(b) shows the edge-preserving smoothed image in Fig. 3(a) by the original guided filter. This image shows the sufficiently smoothed-out edge structures that appeared in the areas that correspond to the dark areas in the original image. However, edge leaks occur in the boundary region separating the dark and bright areas. During image fusion, edge leaks can significantly change the lightness order. To suppress such edge leakage, we introduce adaptive processing to determine ε, which is usually a constant in Eq. (6), for each pixel using $\sigma(i,j)$ as follows:

$$\varepsilon(i,j) = -\frac{\varepsilon_{\max}}{\sigma_{\max}}\cdot\sigma(i,j) + \varepsilon_{\max}, \tag{12}$$

where $\varepsilon(i,j)$ is the value of ε for the pixel at the coordinates (i,j) in I; $\sigma_{\max}$ and $\varepsilon_{\max}$ are the parameters with the maximum values of $\sigma(i,j)$ and $\varepsilon(i,j)$, respectively. Figures 4(a) and 4(b) show the values of σ and ε in grayscale images. In these images, the brighter pixels have larger values of σ and ε. In these figures, $\sigma(i,j)$ values are larger and $\varepsilon(i,j)$ values are smaller in the border region between the dark and bright areas in the original image. On the other hand, $\sigma(i,j)$ is smaller and $\varepsilon(i,j)$ is larger in the region corresponding to the dark areas in the original image. This tendency indicates the following: the edge preservation performance of the guided filter is higher in the dark and bright border region with high contrast and lower in the other regions with low contrast.

Figure 3(c) shows the result of applying the modified guided filter to W introducing Eq. (12). By comparing Figs. 3(b) and 3(c), we can observe that the edge leakage is suppressed. In the proposed method, the filter window width n is set to n_p% of the number of pixels on the input image long side to stabilize the effect of the guided filter without being affected by the image size. The correction process with the guided filter is conducted using the fast arithmetic method based on an integral image proposed by Viola and Jones [40]. This fast computing method can apply the correction in a short computation time of $\mathcal{O}(N)$.

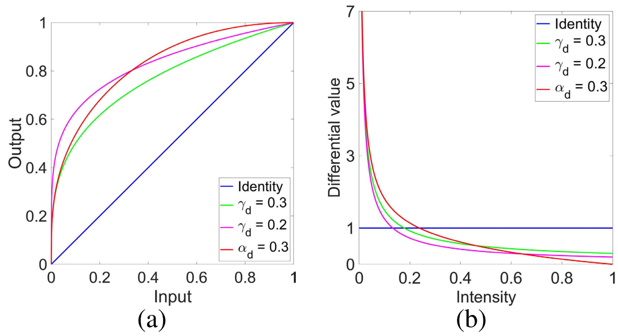

FIGURE 5. Difference between the ordinary and adaptive gamma correction methods with an upward-convex tone curve. (a) Tone curves. (b) Slopes of the curves in (a).

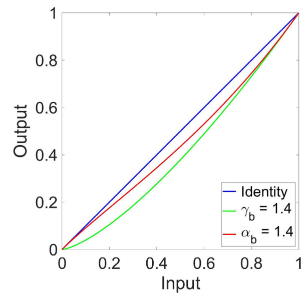

FIGURE 6. Difference between the ordinary and adaptive gamma correction methods using a downward-convex tone curves.

B. GENERATION OF ENHANCED LIGHTNESS IMAGES FOR EACH AREA

To improve the visibility of the dark and bright areas of a backlit image, two lightness-enhanced images are generated from the input lightness image I. In the proposed method, only tone curves are used to generate the enhanced lightness images, improving visibility while maintaining the lightness order in the original image and speeding up the processing.

First, for the dark areas, an adaptive gamma correction using an upward-convex tone curve is applied to generate a lightness-enhanced image G as follows:

$$G(i,j) = (1 - I_{min})\cdot\left(\frac{I(i,j) - I_{min}}{1 - I_{min}}\right)^{\gamma_d(i,j)} + I_{min}, \tag{13}$$

$$\gamma_d(i,j) = \alpha_d\cdot\left(\frac{1 - I(i,j)}{1 - I_{min}}\right), \tag{14}$$

where I_{min} is the minimum lightness in I and α_d is a parameter.

The difference between the adaptive gamma correction represented by Eq. (13) and the ordinary gamma correction with a constant γ_d value is explained using Fig. 5.

Figures 5(a) and 5(b) show the tone curves and their slopes, respectively. The blue line represents the identity transformation; the green and magenta lines represent the gamma correction with $\gamma_d = 0.3$ and $\gamma_d = 0.2$, respectively; the red line represents the adaptive gamma correction with $\alpha_d = 0.3$. In Fig. 5, the tone curves of the ordinary gamma correction have slopes below 1 when the lightness value ranges from 0.1 to 0.2. On the other hand, the slope of the adaptive gamma correction falls below 1 when the lightness value ranges from 0.2 to 0.3. That is, the adaptive gamma transform can increase the lightness of the entire image while amplifying the difference between darkness and lightness over a broader range than the ordinary gamma transform.

Figures 2(d) and 2(e) show an example of a lightness-transformed image G and its lightness histogram, respectively. By comparing Figs. 2(c) and 2(e), we can observe that the lightness differences between pixels with low lightness values are amplified in Fig. 2(e) and the entire distribution shifts to the bright region. On the other hand, there are only a few pixels with lightness values from 0 to 0.2, with the narrowing of the dynamic range remaining as a problem. To address this problem, the S-shaped transformation is applied to the image G to generate an enhanced lightness image E_d as follows:

$$E_d(i,j) = \begin{cases} f^{1-\beta_d} I(i,j)^{\beta_d}, & 0 \leq I(i,j) < f \\ 1-(1-f)^{1-\beta_d}(1-I(i,j))^{\beta_d}, & \text{otherwise}, \end{cases} \tag{15}$$

$$f = \frac{1}{m} \sum_{\{(i,j)|I(i,j)<t\}} G(i,j), \tag{16}$$

where f is the inflection point of the S-shaped tone curve; f is the average of m numbers of pixel values of $G(i,j)$ that satisfy $I(i,j) < t$; β_d is a parameter. Figures 2(f) and 2(g) show an example of an enhanced lightness image for the dark areas E_d and its lightness histogram, respectively. By comparing Figs. 2(d) and 2(f), we can find that the contrast is enhanced in the areas of the person and ground. The difference between the dark and bright areas has increased owing to the broader dynamic range, as shown in Figs. 2(e) and 2(g).

Next, an adaptive gamma transform using a downward-convex tone curve is applied to the lightness image I to generate an enhanced lightness image E_b for the bright areas as follows:

$$E_b(i,j) = I(i,j)^{\gamma_b(i,j)}, \tag{17}$$

$$\gamma_b(i,j) = (\alpha_b - 1) \cdot I(i,j) + 1, \tag{18}$$

where α_b is a parameter. The curves shown in Fig. 6 illustrate the input–output relationship of the gamma correction with a constant value of γ_b and the adaptive gamma correction using Eq. (17). The blue line shows the identity transformation; the green line shows the ordinary gamma correction with $\gamma_b = 1.4$; the red line shows the tone curve of the adaptive gamma correction with $\alpha_b = 1.4$. Figures 2(h) and 2(i) show the lightness image E_b and its lightness histogram with the bright areas enhanced, respectively. These figures show that the adaptive gamma correction amplifies the difference between dark and bright areas with high lightness values while suppressing the decrease in lightness in the mid-range compared with the ordinary gamma correction. This characteristic improves the visibility of the bright areas while suppressing the inversion of the lightness order between the dark and bright areas where the lightness increases owing to the enhancement process. By comparing Figs. 2(b) and 2(h) and focusing on the changes in both the image and the histogram, we can see that the proposed method amplifies the difference between the dark and bright areas with high lightness values.

C. FUSION OF TWO ENHANCED LIGHTNESS IMAGES BASED ON A WEIGHT MAP

The weighted sum of the pixel values at the coordinates (i,j) of the enhanced lightness images E_d and E_b is calculated to obtain the output lightness image O as follows:

$$O(i,j) = \tilde{W}(i,j) \cdot E_d(i,j) + (1 - \tilde{W}(i,j)) \cdot E_b(i,j). \tag{19}$$

In Eq. (19), $O(i,j)$ approaches $E_d(i,j)$ in dark areas as $\tilde{W}(i,j)$ approaches 1. That is, the enhancement effects of the upward-convex adaptive gamma correction and the S-shaped transformation are dominantly reflected in the output image. On the other hand, $O(i,j)$ approaches $E_b(i,j)$ when $\tilde{W}(i,j)$ approaches 0 in the bright areas. That is, the enhancement effect of the adaptive gamma correction using a downward-convex tone curve is dominantly reflected in the output image.

D. CALCULATION OF OUTPUT COLOR IMAGE

After calculating the final output lightness image O, the pixel value at the coordinates (i,j) of the output color image $\boldsymbol{O}^c$ is calculated as follows:

$$\boldsymbol{O}^c(i,j) = \boldsymbol{I}^c(i,j) \cdot \frac{O(i,j)}{I(i,j)}. \tag{20}$$

Figures 2(j) and 2(k) show the output lightness and color images, respectively. These images show that the proposed method effectively improves the visibility of the dark areas without generating artifacts.

III. EXPERIMENTS

A. EXPERIMENTAL CONDITIONS

To demonstrate the effectiveness of the proposed method, comparative experiments were performed using a set of 238 backlit images with bimodal distributions of lightness. This image set contains Creative Commons Zero (CC0) images published on StockSnap.io and flickr.com and the dataset produced by Li [41]. The 238 images are in 24-bit full color and range in size from 44,308 to 1,468,600 pixels. As methods for comparison, CLAHE [5], those developed by Wang et al. [11], Buades et al. [13], Li and Wu [21], Zhang et al. [23], Wang et al. (NPEA) [8], Fu et al. [12], and Guo et al. (LIME) [9] were used. The parameters in the compared methods were set according to each study. Regarding the proposed method, preliminary experiments were conducted by changing each parameter to determine the best ones quantitatively and qualitatively. As a result, the parameters were set to $\alpha_d = 0.3$, $\beta_d = 3.0$, $\alpha_b = 1.4$, $n_p = 10$, $\varepsilon_{max} = 0.5$, and $\sigma_{max} = 0.5$. In the qualitative evaluation by visual inspection, the processing results were compared for 3 of the 238 images showing the characteristics of each method well. In the quantitative evaluation, the LOE [8], [9], [42], Q value [43], and blind image quality measure of enhanced images (BIQME) score [44] were used.

LOE is an index showing the change in the relationship of lightness order between the original image and the processing result. The LOE is calculated as follows:

$$LOE = \frac{1}{M \cdot N} \sum_{i=1}^{M} \sum_{j=1}^{N} RD(i, j), \tag{21}$$

$$RD(x, y) = \sum_{i=1}^{M} \sum_{j=1}^{N} U(L(x, y), (L(i, j)) \oplus U(L_r(x, y), L_r(i, j)), \tag{22}$$

$$U(p, q) = \begin{cases} 1, & p \geq q \\ 0, & \text{otherwise,} \end{cases} \tag{23}$$

where M and N are the numbers of vertical and horizontal pixels in the input image, respectively; $\oplus$ is the exclusive-or operator; and $L(x, y)$ and $L_r(x, y)$ are the maximum values of the RGB components at the coordinates (x, y) in the original and processed images, respectively. The lower the LOE, the better the method in that the lightness order is not disrupted. If the relationship of lightness order between darkness and brightness is disrupted during image enhancement, unnatural light patterns (i.e., artifacts) that did not exist in the original image may appear and cause image quality degradation. The LOE tends to be higher as the number of pixels increases. Therefore, in this experiment, the image size was set to $(M{\cdot}100/\min(M, N), N{\cdot}100/\min(M, N))$. This setting reduces the variation in the number of pixels for each experimental image while preserving the aspect ratio.

The Q value is an index used for evaluating the image quality on the basis of lightness and contrast. In calculating the Q value, first, the input image is divided into blocks of 50×50 pixels without overlap. Then, the overall average of the standard deviations of the pixel values in each block $\overline{\sigma}$ and the average lightness of the image $\overline{I}$ are calculated. The Q value is calculated as follows:

$$Q = \overline{I}\overline{\sigma}. \tag{24}$$

In the proposed method, the original image is divided into dark and bright areas, and enhancement is applied to each area. Therefore, in this evaluation, the original image was divided into dark and bright areas, and Q, $\overline{I}$, and $\overline{\sigma}$ were calculated for each area. Specifically, the original image was divided into 50×50 pixel blocks with no overlap, and the average of pixel values within each block was calculated. The blocks with the lower 10% of the average values were set as the dark area. The blocks with the upper 10% of the average values were set as the bright area.

The BIQME score is an index for calculating the nonreference image quality score based on 17 features related to contrast, sharpness, lightness, colorfulness, and naturalness of the image. The larger the BIMQE score, the better the image quality.

B. EXPERIMENTAL RESULTS AND QUALITATIVE EVALUATION

Figure 7 shows the comparison for various scenes of backlit images. The proposed method shows good enhancement results for the backlit images of various scenes, with no overall over-enhancement or unnatural artifacts. Figures 8, 9, and 10 show three representative processing results and their partially magnified images that show the characteristics of each method well. These images were selected from 238 backlit images, named Images 1, 2, and 3. The details of the experimental results and qualitative evaluation are as follows.

1) RESULTS FOR IMAGE 1

Figure 8 shows the processing results for Image 1. Regarding CLAHE and the methods of Wang and Buades, the visibility of the dark parts is improved without artifacts. However, stripe artifacts occur in the bright areas, and the smoothness of the gradations is impaired. Li's method does not lose smoothness in the brightness gradation in bright areas but causes color smearing on the person and roads. LIME shows a bright result with a slight over-enhancement. In contrast to these methods, NPEA, Zhang's, Fu's, and the proposed methods effectively improve visibility while suppressing artifacts.

2) RESULTS FOR IMAGE 2

Figure 9 shows the processing results for Image 2. Regarding CLAHE and the methods of Wang and Buades, the island visibility at the image center is improved compared with that in the original image. On the other hand, artifacts occur in the bright gradation regions, and the smoothness of the gradient is impaired. Li's method significantly improves the island visibility at the center of the image, but the extreme enhancement of the island alone gives an unnatural impression. Zhang's method causes black clipping in dark areas, resulting in reduced visibility. In contrast to these methods, NPEA, LIME, Fu's, and the proposed methods effectively improve visibility without sacrificing the smoothness of the brightness gradation in the bright areas.

3) RESULTS FOR IMAGE 3

Figure 10 shows the processing results for Image 3. CLAHE and the methods of Wang and Buades significantly improve visibility in dark and bright areas. On the other hand, artifacts and roughness occur around the light source and in brightness gradation in the bright areas. Li's method improves the

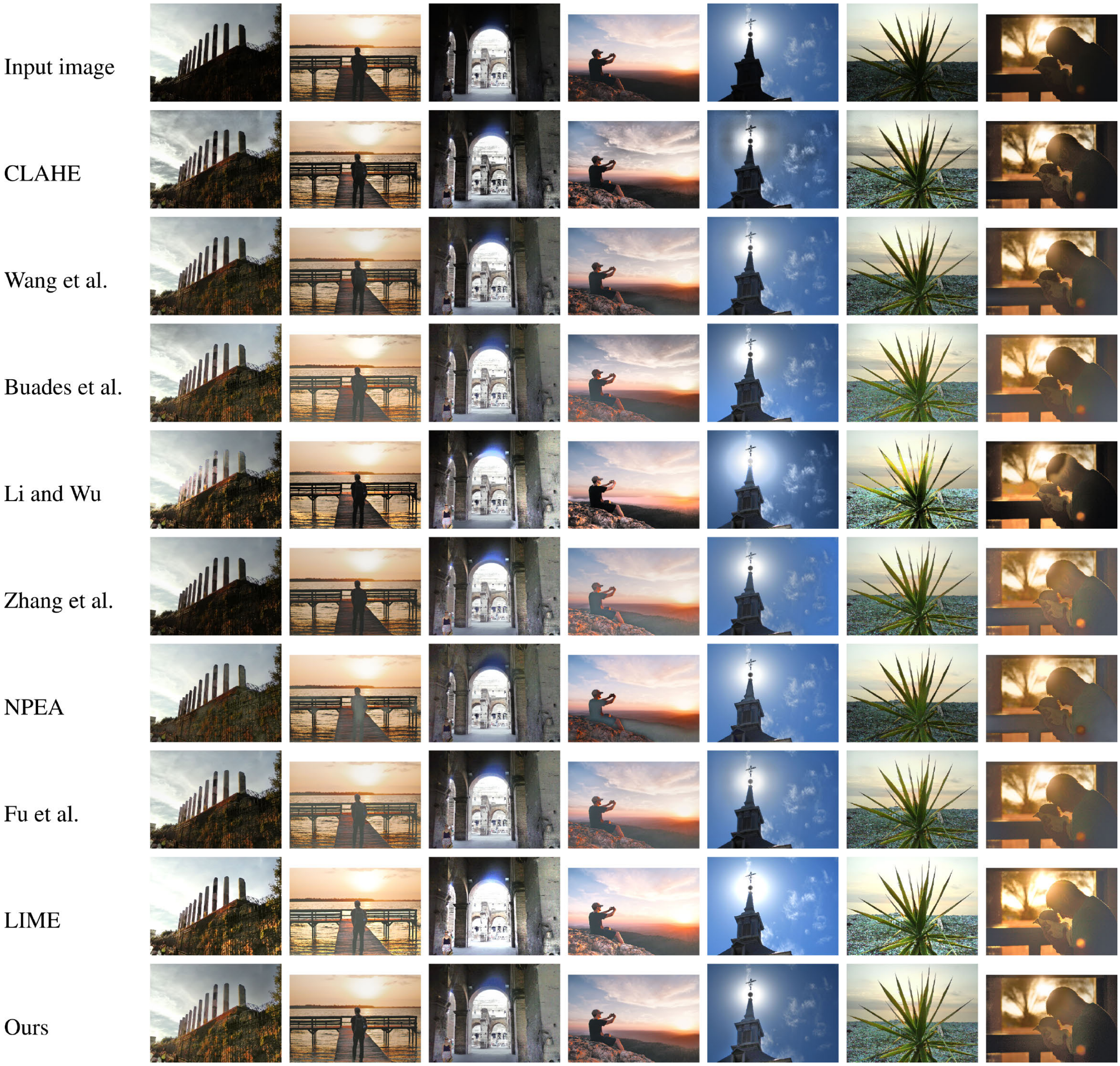

FIGURE 7. Comparison for various backlit images.

visibility of the person, plants, and trees compared with the original image. On the other hand, the light source area in the lower left of the image causes light-induced color smearing. The visibility of the dark areas is hardly improved by Zhang's method. In contrast to these methods, NPEA, LIME, Fu's, and the proposed methods improve visibility in dark and bright areas while suppressing artifacts and roughness.

C. EXPERIMENTAL RESULTS AND QUANTITATIVE EVALUATION

Table 1 shows the averages and standard deviations of LOEs of each method for the 238 images. This table shows the lowest average and standard deviation in bold. The proposed method has the lowest average and standard deviation compared with the other methods. Therefore, the proposed method best preserves the lightness order of the original image and suppresses the occurrence of unnatural artifacts.

The images calculated using Eq. (22) for Images 1, 2, and 3 and their partially magnified images are shown in Figs. 11, 12, and 13, respectively. The closer each pixel is to blue, the lower the RD value; the closer to yellow, the higher the RD value. In CLAHE, Wang's, and Buades' methods, the lightness order changes over a wide image area, including artifacts generated in the bright areas. In Li's method, the lightness order changes markedly in the regions causing color smearing. In Zhang's method, the order of lightness changes

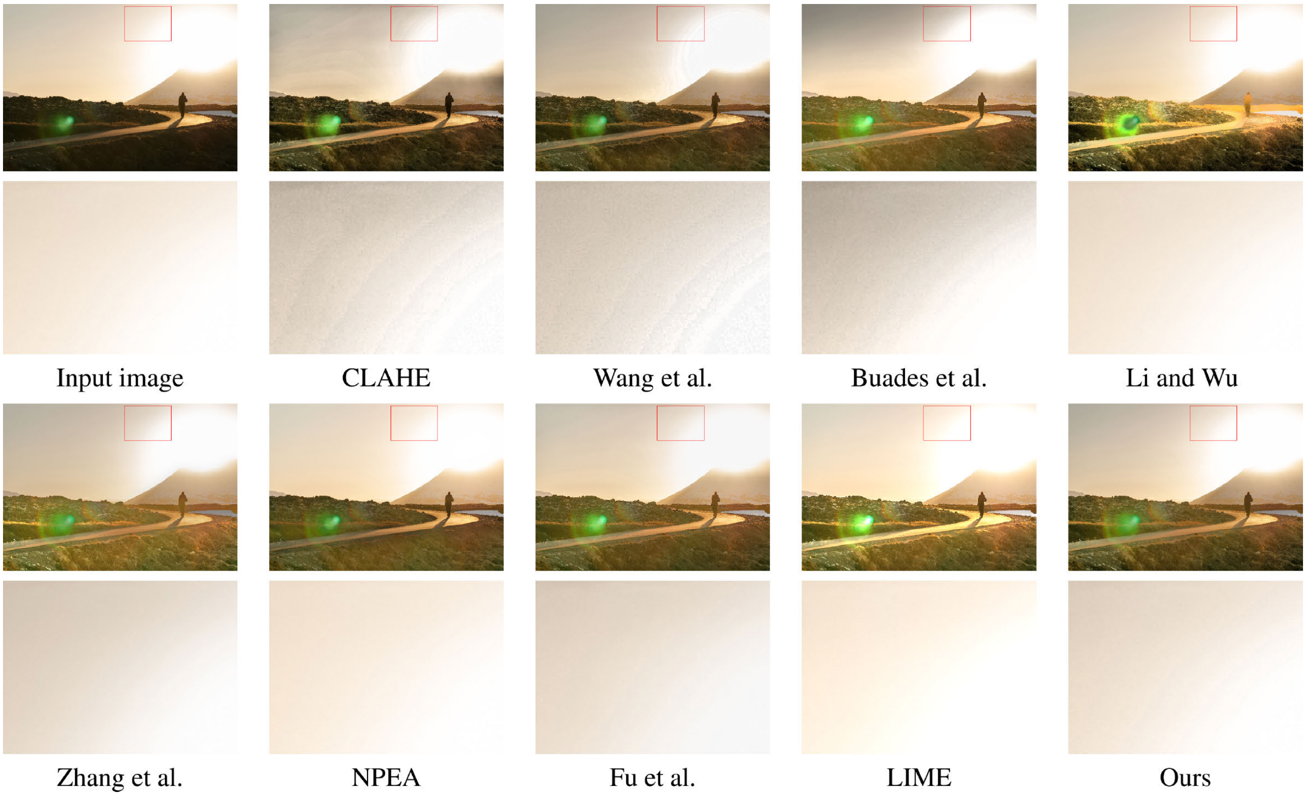

FIGURE 8. Processing results for Image 1. The red rectangles indicate the magnified areas.

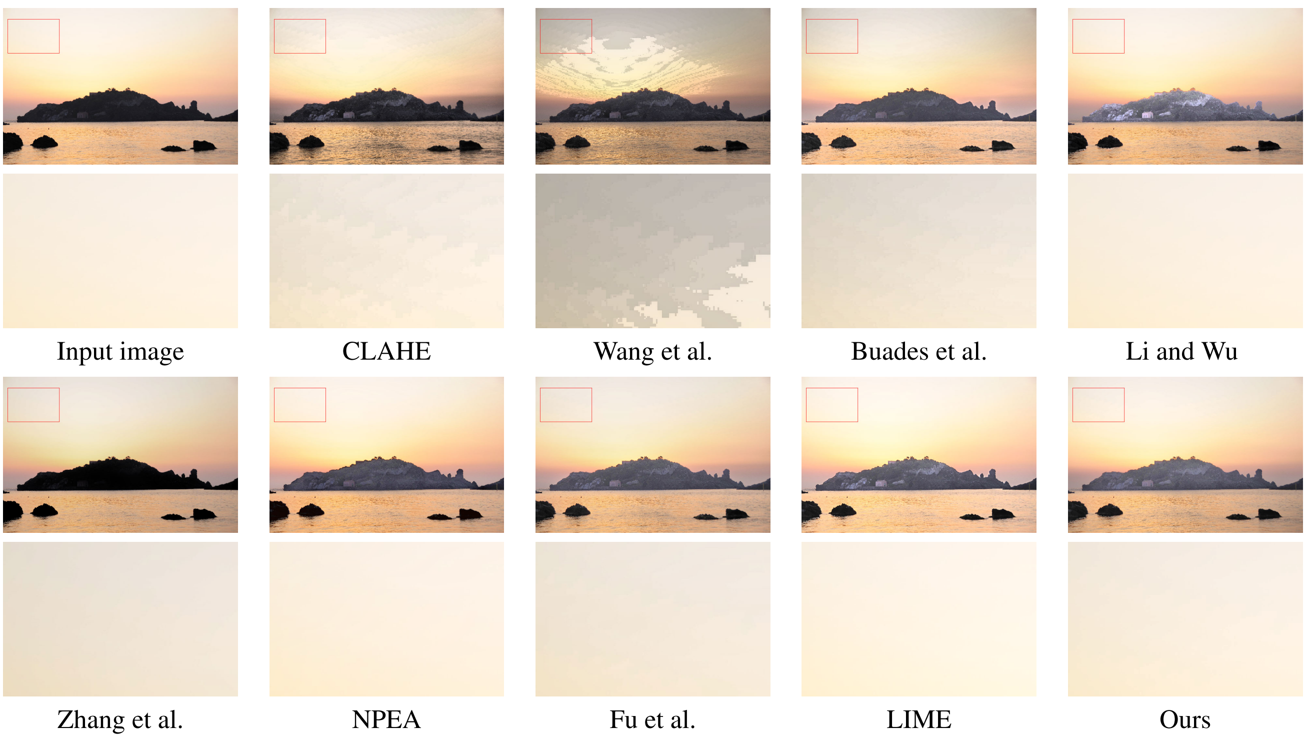

FIGURE 9. Processing results for Image 2. The red rectangles indicate the magnified areas.

over a broad region of bright areas. In LIME, it is evident that the lightness order changes drastically in the bright areas. On the other hand, NPEA, Fu's, and the proposed methods show a much smaller variation in lightness order in the entire

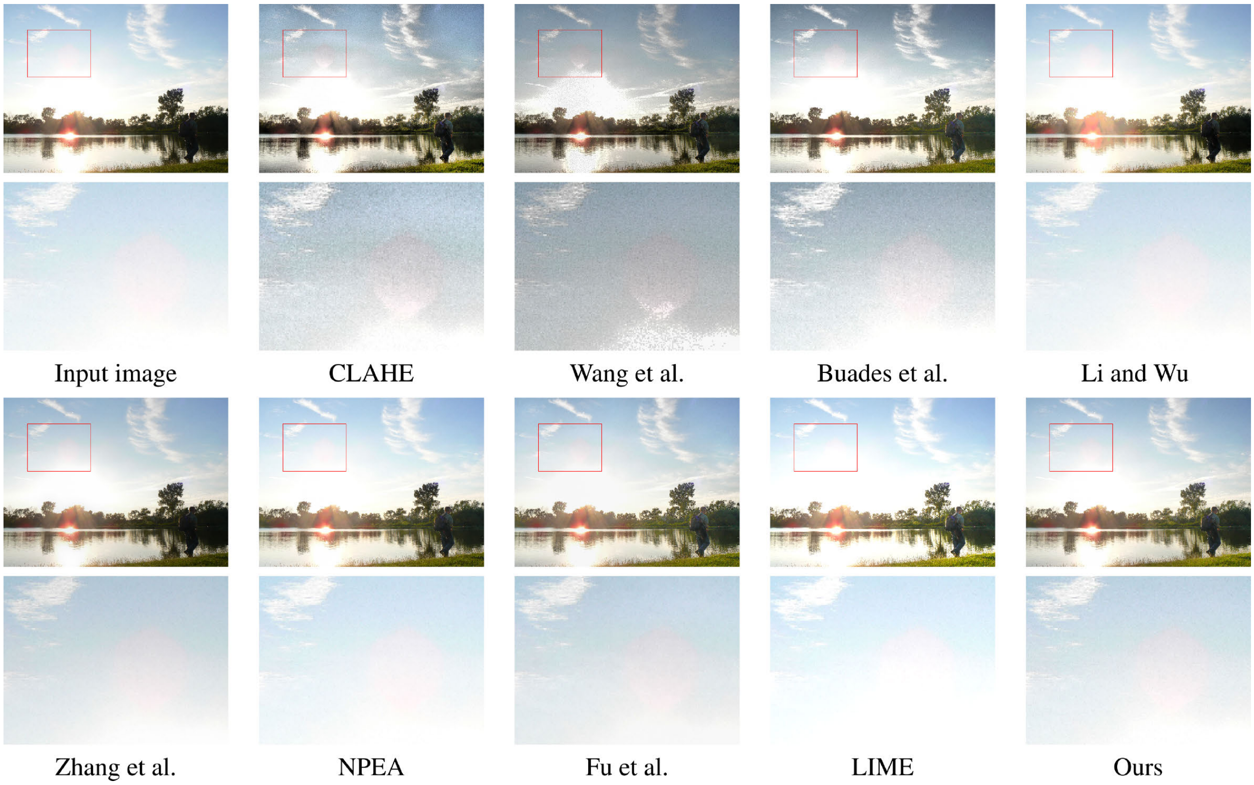

FIGURE 10. Processing results for Image 3. The red rectangles indicate the magnified areas.

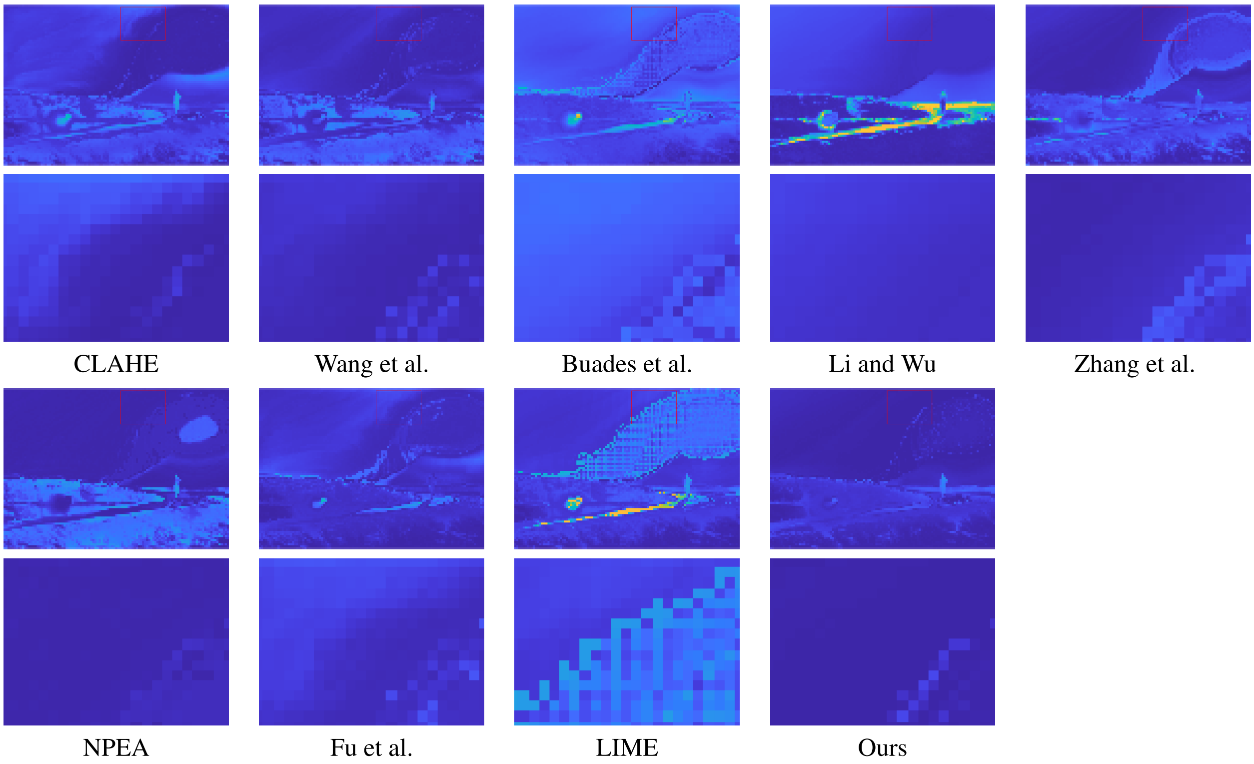

FIGURE 11. Comparison of lightness distortion (RD) in Image 1. The red rectangles indicate the magnified areas.

image than the other methods. Therefore, these methods are less likely to produce unnatural dark and bright artifacts.

Table 2 shows the averages and standard deviations of Q, $\overline{I}$, and $\overline{\sigma}$ for the dark areas in the 238 test images.

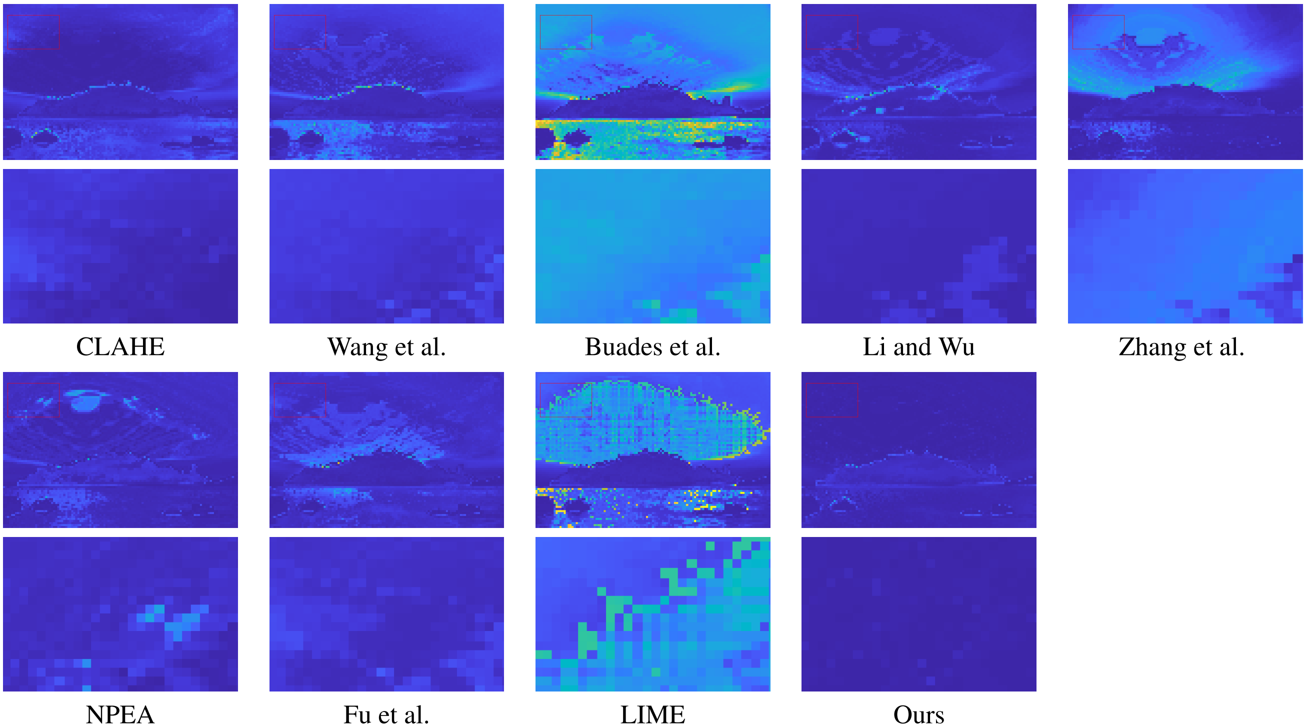

FIGURE 12. Comparison of lightness distortion (RD) in Image 2. The red rectangles indicate the magnified areas.

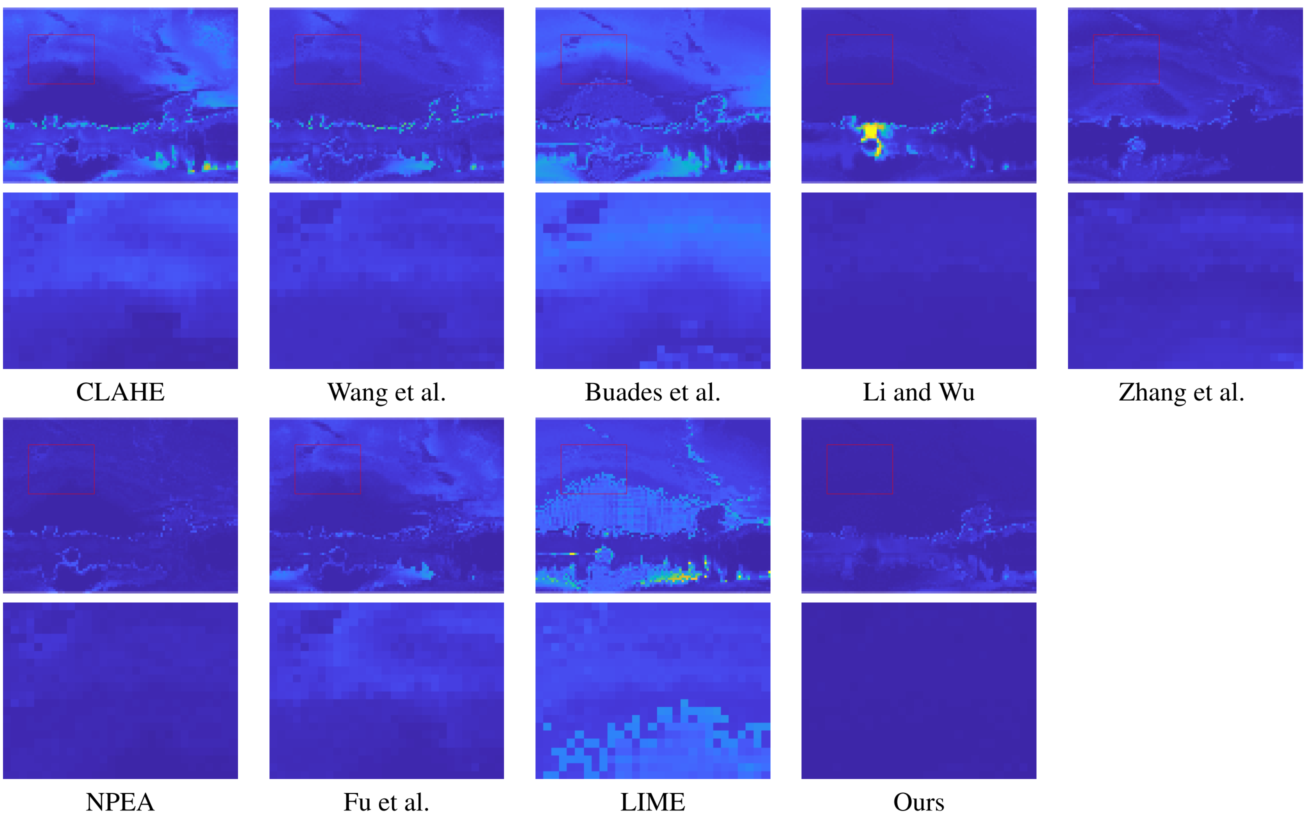

FIGURE 13. Comparison of lightness distortion (RD) in Image 3. The red rectangles indicate the magnified areas.

In Table 2, the highest average and lowest standard deviation are shown in bold. The results show that $\overline{I}$ and $\overline{\sigma}$ are significantly higher, and Q is slightly higher in the proposed method than in the original image. The proposed

FIGURE 14. Changes in processing results when parameters α_d and β_d are varied ($\alpha_b = 1.5$, $n_p = 10$, $\varepsilon_{\max} = 0.5$, and $\sigma_{\max} = 0.5$).

TABLE 1. Comparison of LOEs.

	AVG	SD
CLAHE	1269	499
Wang	961	519
Buades	1538	755
Li	1292	677
Zhang	1172	1035
NPEA	1074	842
Fu	830	471
LIME	1193	371
Ours	**700**	**320**

TABLE 2. Comparison of Q, $\bar{I}$, and $\bar{\sigma}$ for dark areas.

	AVG			SD		
	Q	$\bar{I}$	$\bar{\sigma}$	Q	$\bar{I}$	$\bar{\sigma}$
Input	393	24.1	11.1	**813**	**18.3**	11.8
CLAHE	1119	39.9	22.6	1407	19.8	14.6
Wang	1123	52.0	20.7	874	20.0	11.5
Buades	1508	68.5	21.5	1254	28.4	13.0
Li	1647	46.0	**28.8**	1708	26.9	16.6
Zhang	1648	69.6	22.4	1390	40.5	14.7
NPEA	1307	68.5	19.8	904	23.4	**10.9**
Fu	1287	62.3	20.0	1105	31.5	12.2
LIME	**2201**	**75.3**	28.2	1785	33.7	16.6
Ours	1541	57.9	25.2	1135	22.0	12.3

method also has relatively higher $\bar{\sigma}$ than the compared methods.

Table 3 shows the averages and standard deviations of Q, $\bar{I}$, and $\bar{\sigma}$ for the bright areas. In Table 3, the highest average and lowest standard deviation are shown in bold. The results show that Q is lower in NPEA, LIME, Li's, Zhang's, and Fu's methods owing to the decrease in $\bar{\sigma}$ than in the original image. On the other hand, CLAHE, Wang's, and Buades', and the proposed methods have higher Q values owing to the increase in $\bar{\sigma}$. These results show that the proposed method has relatively high visibility improvement in both dark and bright areas.

Table 4 shows the averages and standard deviations of the BIQME scores for the methods. In Table 4, the highest average and lowest standard deviation are shown in bold. The calculation results show that the proposed method has relatively higher values than the compared methods. The BIQME scores show that the images processed by the proposed method have relatively good quality.

From the results of LOE, Q-value, and BIQME score, it can be confirmed that the compared methods improve visibility while markedly changing the orders of darkness and lightness. On the other hand, the proposed method tends to keep the orders of darkness and lightness in the original image the same. It is highly effective in improving visibility while suppressing the occurrence of artifacts.

Table 5 shows the average calculation times of the methods for 238 experimental images. This table shows the shortest average time and standard deviation in bold. In this regard, because we used the online code in Buades' method, there is no measurement result. The execution environment is as follows: CPU, Intel®Core™ i9-13900KF 3.00 GHz; memory, 64.0GB; OS, Windows 11 Pro; and programming language, Python 3.10.11 (Zhang et al.) and MATLAB R2023a (the others). Table 5 shows that although it is inferior

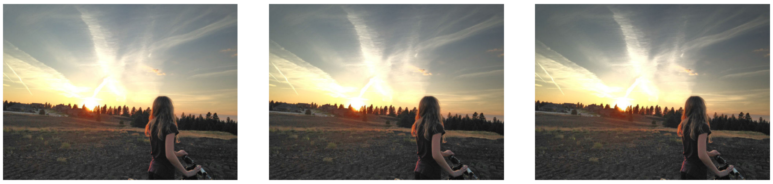

FIGURE 15. Changes in processing results when parameter α_b is varied ($\alpha_d = 0.5$, $\beta_d = 2.0$, $n_p = 10$, $\varepsilon_{max} = 0.5$, $\sigma_{max} = 0.5$).

TABLE 3. Comparison of Q, $\bar{I}$, and $\bar{\sigma}$ for bright areas.

	AVG			SD		
	Q	$\bar{I}$	$\bar{\sigma}$	Q	$\bar{I}$	$\bar{\sigma}$
Input	2650	236.0	12.0	2745	17.5	13.4
CLAHE	**3890**	222.6	**18.9**	2860	24.5	15.5
Wang	3123	230.4	14.1	2532	17.0	12.4
Buades	3246	238.9	14.1	2753	14.6	12.8
Li	2343	237.4	10.4	2320	15.6	11.1
Zhang	2403	229.1	10.9	**2295**	16.3	**10.9**
NPEA	2454	240.7	10.8	2642	14.2	12.5
Fu	2520	233.1	11.3	2387	13.8	11.4
LIME	1838	**250.8**	7.6	2611	**7.0**	11.1
Ours	2688	232.2	12.3	2428	19.6	11.9

TABLE 4. Comparison of BIQME scores.

	AVG	SD
Input	0.560	0.0556
CLAHE	**0.603**	0.0420
Wang	0.598	0.0452
Buades	0.568	0.0619
Li	0.600	**0.0393**
Zhang	0.542	0.0709
NPEA	0.578	0.0558
Fu	0.565	0.0682
LIME	0.570	0.0702
Ours	0.588	0.0450

to CLAHE and LIME, the proposed method is relatively fast considering the image quality obtained in the qualitative and quantitative evaluations. The analysis of the processing revealed that the edge-preserving smoothing process was the bottleneck. Therefore, further improvements in this processing and implementation using a faster programming language are needed to reduce the processing time in future work.

As a result of the above experiments, it is confirmed that the proposed method can suppress unnatural dark and bright artifacts and sufficiently improve visibility in a relatively short computation time.

D. BEHAVIOR OF THE PROPOSED METHOD FOR VARYING PARAMETERS

Figure 14 shows the processing effect of the proposed method for the parameters α_d and β_d. The other parameters were set as follows: $\alpha_b = 1.5$, $n_p = 10$, $\varepsilon_{max} = 0.5$, and $\sigma_{max} = 0.5$.

TABLE 5. Comparison of average processing times (in sec).

	AVG	SD
CLAHE	**0.009**	**0.003**
Wang	0.090	0.029
Buades	-	-
Li	32.13	40.40
Zhang	27.58	0.257
NPEA	3.479	1.248
Fu	0.077	0.026
LIME	0.026	0.010
Ours	0.048	0.018

Figure 14 shows that as α_d decreases, the person and ground at the bottom of the image become brighter. On the other hand, as β_d increases, the contrast between dark areas, such as the person and ground, increases.

Figure 15 shows the processing effect of the proposed method for the parameter α_b. The other parameters were set as follows: $\alpha_d = 0.5$, $\beta_d = 2.0$, $n_p = 10$, $\varepsilon_{max} = 0.5$, and $\sigma_{max} = 0.5$. Figure 15 shows that as α_b increases, the contrast of the clouds in the upper part of the image, which corresponds to the bright area, increases.

IV. CONCLUSION

In this paper, we proposed a fast backlit image enhancement method that can suppress the LOE and the generation of artifacts. In the proposed method, two lightness images, in which dark and bright areas are separately enhanced by tone curve processing, are fused on the basis of a weight map, and the output lightness is calculated. The weight map used in the fusion process is generated using Otsu's binarization method and a modified guided filter with adaptive processing. By weighting the dark areas using these methods, edge leakage in the dark and bright boundary regions is suppressed while considering the original image's local dark and bright patterns. The effect of this process is to suppress the LOE in the enhancement process.

To verify the effectiveness of the proposed method, we conducted experiments to compare our proposed method with the conventional methods using multiple backlit images. In the experiments, qualitative and quantitative evaluations were conducted. The experimental results show that the proposed method significantly improves the visibility of dark and bright areas in backlit images while suppressing the generation of artifacts by reducing the LOE. Furthermore, a comparison of the average computation time among the methods confirms that the proposed method is relatively fast, considering the resulting image quality.

One of the potential limitations is that the proposed method assumes that the lightness histogram in backlit images is bimodal; sufficient enhancement effects may not be obtained in low-light images where this assumption does not hold or only has weak bimodality. Furthermore, although there are problems with the implementation method, environment, and programming language, it is necessary to improve the proposed algorithm to an essentially faster one that can process larger images in real time. Given the potential limitations mentioned above, as future works, we are considering developing an automatic and adaptive parameter adjustment method and a faster backlit image enhancement method specifically for movies.

REFERENCES

[1] S. Battiato, G. Messina, and A. Castorina, "Exposure correction for imaging devices: An overview," in *Single-Sensor Imaging: Methods and Applications for Digital Cameras*, R. Lukac, Ed. Boca Raton, FL, USA: CRC Press, 2009, ch. 12, pp. 336–337.

[2] M. Li, J. Liu, W. Yang, X. Sun, and Z. Guo, "Structure-revealing low-light image enhancement via robust retinex model," *IEEE Trans. Image Process.*, vol. 27, no. 6, pp. 2828–2841, Jun. 2018, doi: 10.1109/TIP.2018.2810539.

[3] R. Al Sobbahi and J. Tekli, "Low-light homomorphic filtering network for integrating image enhancement and classification," *Signal Process., Image Commun.*, vol. 100, Jan. 2022, Art. no. 116527, doi: 10.1016/j.image.2021.116527.

[4] Y. Zhu, X. Fu, and A. Liu, "Learning dual transformation networks for image contrast enhancement," *IEEE Signal Process. Lett.*, vol. 27, pp. 1999–2003, 2020, doi: 10.1109/LSP.2020.3036312.

[5] K. Zuiderveld, "Contrast limited adaptive histogram equalization," in *Graphics Gems IV*. New York, NY, USA: Academic, 1994, pp. 474–485.

[6] D. J. Jobson, Z. Rahman, and G. A. Woodell, "Properties and performance of a center/surround retinex," *IEEE Trans. Image Process.*, vol. 6, no. 3, pp. 451–462, Mar. 1997, doi: 10.1109/83.557356.

[7] D. J. Jobson, Z. Rahman, and G. A. Woodell, "A multiscale retinex for bridging the gap between color images and the human observation of scenes," *IEEE Trans. Image Process.*, vol. 6, no. 7, pp. 965–976, Jul. 1997, doi: 10.1109/83.597272.

[8] S. Wang, J. Zheng, H.-M. Hu, and B. Li, "Naturalness preserved enhancement algorithm for non-uniform illumination images," *IEEE Trans. Image Process.*, vol. 22, no. 9, pp. 3538–3548, Sep. 2013, doi: 10.1109/TIP.2013.2261309.

[9] X. Guo, Y. Li, and H. Ling, "LIME: Low-light image enhancement via illumination map estimation," *IEEE Trans. Image Process.*, vol. 26, no. 2, pp. 982–993, Feb. 2017, doi: 10.1109/TIP.2016.2639450.

[10] J. S. Park, J. W. Soh, and N. I. Cho, "Generation of high dynamic range illumination from a single image for the enhancement of undesirably illuminated images," *Multimedia Tools Appl.*, vol. 78, no. 14, pp. 20263–20283, Feb. 2019, doi: 10.1007/s11042-019-7384-z.

[11] Q. Wang, X. Fu, X.-P. Zhang, and X. Ding, "A fusion-based method for single backlit image enhancement," in *Proc. IEEE Int. Conf. Image Process. (ICIP)*, Phoenix, AZ, USA, Sep. 2016, pp. 4077–4081, doi: 10.1109/ICIP.2016.7533126.

[12] X. Fu, D. Zeng, Y. Huang, Y. Liao, X. Ding, and J. Paisley, "A fusion-based enhancing method for weakly illuminated images," *Signal Process.*, vol. 129, pp. 82–96, Dec. 2016, doi: 10.1016/j.sigpro.2016.05.031.

[13] A. Buades, J. Lisani, A. B. Petro, and C. Sbert, "Backlit images enhancement using global tone mappings and image fusion," *IET Image Process.*, vol. 14, no. 2, pp. 211–219, Feb. 2020, doi: 10.1049/iet-ipr.2019.0814.

[14] P. Burt and E. Adelson, "The Laplacian pyramid as a compact image code," *IEEE Trans. Commun.*, vol. COM-31, no. 4, pp. 532–540, Apr. 1983, doi: 10.1109/TCOM.1983.1095851.

[15] G. Deng, "A generalized unsharp masking algorithm," *IEEE Trans. Image Process.*, vol. 20, no. 5, pp. 1249–1261, May 2011, doi: 10.1109/TIP.2010.2092441.

[16] T. Mertens, J. Kautz, and F. Van Reeth, "Exposure fusion," in *Proc. 15th Pacific Conf. Comput. Graph. Appl. (PG)*, Maui, HI, USA, Oct. 2007, pp. 382–390, doi: 10.1109/PG.2007.17.

[17] Z. Li, K. Cheng, and X. Wu, "Soft binary segmentation-based backlit image enhancement," in *Proc. IEEE 17th Int. Workshop Multimedia Signal Process. (MMSP)*, Xiamen, China, Oct. 2015, pp. 1–5, doi: 10.1109/MMSP.2015.7340808.

[18] J. Vazquez-Corral, P. Cyriac, and M. Bertalmío, "Perceptually-based restoration of backlit images," in *Proc. IST 26th Color Imag. Conf.*, Nov. 2018, vol. 26, no. 1, pp. 32–37, doi: 10.2352/ISSN.2169-2629.2018.26.32.

[19] T. Trongtirakul, W. Chiracharit, and S. S. Agaian, "Single backlit image enhancement," *IEEE Access*, vol. 8, pp. 71940–71950, 2020, doi: 10.1109/ACCESS.2020.2987256.

[20] P. Cyriac, D. Kane, and M. Bertalmío, "Optimized tone curve for in-camera image processing," *Electron. Imag.*, vol. 28, no. 13, pp. 1–7, Feb. 2016, doi: 10.2352/ISSN.2470-1173.2016.13.IQSP-012.

[21] Z. Li and X. Wu, "Learning-based restoration of backlit images," *IEEE Trans. Image Process.*, vol. 27, no. 2, pp. 976–986, Feb. 2018, doi: 10.1109/TIP.2017.2771142.

[22] X. Lv, S. Zhang, Q. Liu, H. Xie, B. Zhong, and H. Zhou, "BacklitNet: A dataset and network for backlit image enhancement," *Comput. Vis. Image Understand.*, vol. 218, Apr. 2022, Art. no. 103403, doi: 10.1016/j.cviu.2022.103403.

[23] L. Zhang, L. Zhang, X. Liu, Y. Shen, S. Zhang, and S. Zhao, "Zero-shot restoration of back-lit images using deep internal learning," in *Proc. 27th ACM Int. Conf. Multimedia*, New York, NY, USA, Oct. 2019, pp. 1623–1631, doi: 10.1145/3343031.3351069.

[24] C. Guo, C. Li, J. Guo, C. C. Loy, J. Hou, S. Kwong, and R. Cong, "Zero-reference deep curve estimation for low-light image enhancement," in *Proc. IEEE/CVF Conf. Comput. Vis. Pattern Recognit. (CVPR)*, Jun. 2020, pp. 1780–1789.

[25] C. Li, C. Guo, and C. C. Loy, "Learning to enhance low-light image via zero-reference deep curve estimation," *IEEE Trans. Pattern Anal. Mach. Intell.*, vol. 44, no. 8, pp. 4225–4238, Aug. 2022, doi: 10.1109/TPAMI.2021.3063604.

[26] C. Li, C. Guo, L. Han, J. Jiang, M.-M. Cheng, J. Gu, and C. C. Loy, "Low-light image and video enhancement using deep learning: A survey," *IEEE Trans. Pattern Anal. Mach. Intell.*, vol. 44, no. 12, pp. 9396–9416, Dec. 2022, doi: 10.1109/TPAMI.2021.3126387.

[27] N. Jiang, J. Lin, T. Zhang, H. Zheng, and T. Zhao, "Low-light image enhancement via stage-transformer-guided network," *IEEE Trans. Circuits Syst. Video Technol.*, vol. 33, no. 8, pp. 3701–3712, Aug. 2023, doi: 10.1109/TCSVT.2023.3239511.

[28] H. Cui, J. Li, Z. Hua, and L. Fan, "Progressive dual-branch network for low-light image enhancement," *IEEE Trans. Instrum. Meas.*, vol. 71, pp. 1–18, 2022, doi: 10.1109/TIM.2022.3216880.

[29] K. G. Lore, A. Akintayo, and S. Sarkar, "LLNet: A deep autoencoder approach to natural low-light image enhancement," *Pattern Recognit.*, vol. 61, pp. 650–662, Jan. 2017, doi: 10.1016/j.patcog.2016.06.008.

[30] C. Wei and W. Wang, W. Yang, and J. Liu, "Deep retinex decomposition for low-light enhancement," in *Proc. Brit. Mach. Vis. Conf.*, 2018, pp. 1–12.

[31] W. Ren, S. Liu, L. Ma, Q. Xu, X. Xu, X. Cao, J. Du, and M.-H. Yang, "Low-light image enhancement via a deep hybrid network," *IEEE Trans. Image Process.*, vol. 28, no. 9, pp. 4364–4375, Sep. 2019, doi: 10.1109/TIP.2019.2910412.

[32] Z. Ni, W. Yang, H. Wang, S. Wang, L. Ma, and S. Kwong, "Cycle-interactive generative adversarial network for robust unsupervised low-light enhancement," in *Proc. 30th ACM Int. Conf. Multimedia*, Oct. 2022, pp. 1484–1492, doi: 10.1145/3503161.3548006.

[33] Z. Zhang, H. Zheng, R. Hong, M. Xu, S. Yan, and M. Wang, "Deep color consistent network for low-light image enhancement," in *Proc. IEEE/CVF Conf. Comput. Vis. Pattern Recognit. (CVPR)*, Jun. 2022, pp. 1899–1908.

[34] W. Wang, Z. Chen, and X. Yuan, "Simple low-light image enhancement based on Weber–Fechner law in logarithmic space," *Signal Process., Image Commun.*, vol. 106, Aug. 2022, Art. no. 116742, doi: 10.1016/j.image.2022.116742.

[35] H. Huang, W. Yang, Y. Hu, J. Liu, and L.-Y. Duan, "Towards low light enhancement with RAW images," *IEEE Trans. Image Process.*, vol. 31, pp. 1391–1405, 2022, doi: 10.1109/TIP.2022.3140610.
[36] M. Cotogni and C. Cusano, "TreEnhance: A tree search method for low-light image enhancement," *Pattern Recognit.*, vol. 136, Apr. 2023, Art. no. 109249, doi: 10.1016/j.patcog.2022.109249.
[37] N. Otsu, "A threshold selection method from gray-level histograms," *IEEE Trans. Syst., Man, Cybern.*, vol. SMC-9, no. 1, pp. 62–66, Jan. 1979, doi: 10.1109/TSMC.1979.4310076.
[38] K. He, J. Sun, and X. Tang, "Guided image filtering," *IEEE Trans. Pattern Anal. Mach. Intell.*, vol. 35, no. 6, pp. 1397–1409, Jun. 2013, doi: 10.1109/TPAMI.2012.213.
[39] J. Shin, H. Oh, K. Kim, and K. Kang, "Automatic image enhancement for under-exposed, over-exposed, or backlit images," in *Proc. IST Int. Symp. Electron. Imag., Color Imag. XXIV, Displaying, Process., Hardcopy, Appl.*, 2019, pp. 88-1–88-6, doi: 10.2352/ISSN.2470-1173.2019.14.COLOR-088.
[40] P. Viola and M. J. Jones, "Robust real-time face detection," *Int. J. Comput. Vis.*, vol. 57, no. 2, pp. 137–154, May 2004, doi: 10.1023/B:VISI.0000013087.49260.fb.
[41] Z. Li. *Li's Database*. Accessed: Sep. 21, 2023. [Online]. Available: https://github.com/7thChord/backlit
[42] Z. Ying, G. Li, Y. Ren, R. Wang, and W. Wang, "A new low-light image enhancement algorithm using camera response model," in *Proc. IEEE Int. Conf. Comput. Vis. Workshops (ICCVW)*, Venice, Italy, Oct. 2017, pp. 3015–3022, doi: 10.1109/ICCVW.2017.356.
[43] D. J. Jobson, Z. Rahman, and G. A. Woodell, "Statistics of visual representation," *Proc. SPIE*, vol. 4736, pp. 25–35, Jul. 2002, doi: 10.1117/12.477589.
[44] K. Gu, D. Tao, J.-F. Qiao, and W. Lin, "Learning a no-reference quality assessment model of enhanced images with big data," *IEEE Trans. Neural Netw. Learn. Syst.*, vol. 29, no. 4, pp. 1301–1313, Apr. 2018, doi: 10.1109/TNNLS.2017.2649101.

MASATO AKAI received the B.S. and M.S. degrees from Yamaguchi University, Japan, in 2021 and 2023, respectively. He is currently an Engineer with the Imaging Solution Development Department, Nikon Corporation, Japan. His research interests include image enhancement and image restoration.

YOSHIAKI UEDA (Member, IEEE) received the M.S. and Ph.D. degrees from Yamaguchi University, Japan, in 2016 and 2019, respectively. He is currently an Associate Professor with the Faculty of Advanced Science and Technology, Ryukoku University, Japan. His research interests include image enhancement and color quantization. He is a member of IEICE.

TAKANORI KOGA (Member, IEEE) received the M.E. and Ph.D. degrees from the Kyushu Institute of Technology, Japan, in 2004 and 2007, respectively. He is currently an Associate Professor with the Faculty of Humanity-Oriented Science and Engineering, Kindai University, Japan. His research interests include image processing, intelligent systems, and interactive systems. He is a member of ACM and IEICE.

NORIAKI SUETAKE (Member, IEEE) received the B.E., M.E., and Ph.D. degrees in control engineering and science from the Kyushu Institute of Technology, Japan, in 1992, 1994, and 2000, respectively. He is currently a Professor with the Graduate School of Sciences and Technology for Innovation, Yamaguchi University, Japan. His research interests include digital signal processing, image processing, and intelligent systems. He is a member of OSA and IEICE.